

Catalytic consequences of micropore topology, mesoporosity, and acidity on the hydrolysis of sucrose over zeolite catalysts†

Cite this: DOI: 10.1039/c4cy00360h

Yao He,^{ab} Thomas C. Hoff,^a Laleh Emdadi,^a Yiqing Wu,^a Judicael Bouraima^a and Dongxia Liu^{*a}

The effects of zeolite micropore topology, mesoporosity, and acidity on the hydrolysis of polysaccharides were probed in reactions of sucrose over a variety of zeolite catalysts (FER, MFI, MOR, MWW, BEA, FAU, pillared MFI (PMFI), and pillared MWW (PMWW)). The measured rate of sucrose hydrolysis over microporous zeolites varied by a factor of ~100 following a trend of FER < MOR ~ MFI < BEA ~ MWW < FAU, indicating that the hydrolysis of sucrose increases with increasing zeolite micropore sizes. The presence of mesoporosity in PMFI and PMWW zeolites enhanced the rates of sucrose reactions by a factor of ~2 in comparison with the microporous MWW and MFI zeolites, which may result from the enhanced acid site accessibility and mitigated diffusion constraints. The examination on the effects of zeolite acidity on the hydrolysis of sucrose by employing MFI, PMFI, BEA, MWW, and FAU zeolites with a range of Si/Al ratios showed that a Si/Al ratio of ~70–150 provides a maximal rate constant per acid site in the catalysts. The measured activation energies of the catalytic reactions in all zeolites were similar. The measured entropies, however, increased abruptly with increasing micropore sizes of zeolites and slightly with increasing mesoporosity in the zeolites. The present study suggests that the hydrolysis of sucrose is driven primarily by the reaction entropies that are dominated consecutively by the micropore topology, acidity, and mesoporosity of the zeolite catalysts.

Received 22nd March 2014,
Accepted 2nd May 2014

DOI: 10.1039/c4cy00360h

www.rsc.org/catalysis

1. Introduction

The dwindling crude oil reserves and environmental issues drive the research for alternative fuel and chemical sources that are currently derived from petroleum.^{1,2} Biomass attracts considerable attention as a renewable feedstock due to its huge reservoir of renewable carbon and “CO₂ moderate” impact on the environment.^{3,4} Sucrose biomass constitutes the main carbohydrate reserve in plant biomass.⁵ The hydrolysis of sucrose allows its conversion into glucose and

fructose sugars, representing the starting point for the synthesis of chemicals or fuels by acid-catalyzed reactions from polysaccharides.^{3,6}

Enzymes,^{7–9} mineral acids,^{10,11} and solid acids^{4,12–17} have been employed as catalysts for the hydrolysis of sucrose. The sucrose conversion over enzyme catalysts is generally efficient, several times faster than with mineral or solid acids. The enzyme stability and narrow operating temperature range, however, are barriers in the enzymatic hydrolysis of sucrose.^{18,19} The homogeneous mineral acids catalyze sucrose conversion in a wide temperature range, while the considerable energy consumption in the product separation, formation of large amount of acid waste, and corrosion problems are the main drawbacks. The development of efficient, easily separable, and environmentally friendly solid acid catalysts is therefore considered for the sucrose hydrolysis reaction. Acid ion-exchange resins,^{12,20–22} polyheteroacids,¹⁵ layered transition-metal oxides,²³ organic–inorganic hybrid sulfonic mesoporous silicas or carbons,^{12,13,24} proton-form zeolites,^{22,25–28} *etc.* have been used as solid acids in the sucrose hydrolysis reactions. The heterogeneous solid acid catalyst systems, however, show concerns on their microenvironment that lead to the diffusion constraint on reactants/products and restricted

^a Department of Chemical and Biomolecular Engineering, University of Maryland, College Park, MD, 20742, USA. E-mail: liud@umd.edu; Fax: +1 301 405 0523; Tel: +1 301 405 3522

^b Institute of Clean Energy Utilization, School of Electric Power, South China University of Technology, Guangzhou, 510640, China

† Electronic supplementary information (ESI) available: Rate constants of hydrolysis of sucrose in zeolites with variable micropore topology, mesoporosity, and acidity (Si/Al ratio); plots for sucrose conversion as a function of reaction time and rate constant determination for sucrose hydrolysis reactions over each catalyst; and plots for determination of measured activation energy and entropy in sucrose hydrolysis reactions over zeolite catalysts. See DOI: 10.1039/c4cy00360h

accessibility to acid sites, considering that the dimensions of sucrose molecules are relatively big (kinetic diameter of ~0.88 nm).^{28–30}

Zeolites are crystalline microporous aluminosilicates, with channel and pocket dimensions typically less than 1 nm, which enable shape-selective catalysis and thus are good candidates for selective conversions of biomass-derived products.³¹ The zeolite topology can promote reaction rates and selectivity based on spatial constraints and attractive or repulsive interactions between adsorbed molecules and pore walls and by altering the relative stability of surface-bound intermediates inside micropores. Meso-/microporous zeolites contain both meso- and micropores, which allow the facile pore access and fast transport of bulky molecules and thereby enable beneficial effects on the activity, selectivity, and/or stability in a wide range of catalyzed reactions.^{32–35} Studies of sucrose hydrolysis have been conducted on faujasite (FAU), beta polymorph A (BEA), mordenite (MOR), and mordenite framework inverted (MFI) structure type zeolites.^{26,28,30,36,37} Moreau *et al.*²⁶ reported that FAU is the most efficient zeolite catalyst in the reactions. Studies on the dealuminated FAU catalysts by Buttersack *et al.*²⁸ showed that two or less protons per unit cell in FAU have the maximum activity per acid site. A systematic study on the zeolite microenvironment (micropore topology, mesoporosity, and acidity) effects of the conventional microporous zeolites and the emerging meso-/microporous zeolites on the sucrose hydrolysis reaction has not been reported.

In the present study, we assessed the catalytic consequences of micropore topology, mesoporosity, and acidity of a range of microporous and meso-/microporous zeolite catalysts on the hydrolysis of sucrose. The commercially available zeolite catalysts, ferrierite (FER), MOR, BEA, MFI, and FAU with a range of Si/Al ratios, were employed to examine the effects of zeolite micropore topology and acidity on the sucrose hydrolysis reactions. The effect of mesoporosity on the sucrose hydrolysis reactions was investigated by using the meso-/microporous pillared MWW (PMWW) and pillared MFI (PMFI) zeolite catalysts. PMWW, derived from a layered precursor, MWW (P), is the first pillared zeolite material with microporous layers and mesoporous interlayer spaces.^{38–41} The synthesis of PMWW was done by expanding layers of MWW (P) by using a surfactant and then intercalating by silica species which converted into inorganic pillars upon condensation and hold the layers apart creating interlayer mesopores. PMFI is a material reported in recent years, which was created by pillaring the multilamellar MFI nanosheets by silica-based species using a similar procedure to that of PMWW.^{42,43} Our previous study showed that the intrinsic catalytic behavior of Brønsted acid sites in the meso-/microporous PMWW and PMFI zeolites is similar to their microporous analogues in the ethanol dehydration and monomolecular conversion of propane and isobutane as probe reactions,⁴⁴ while they showed much efficient catalysis in diffusion constrained catalytic reactions when the self-etherification of benzyl alcohol and alkylation of mesitylene were used as the probe reactions.⁴⁵ The catalytic consequences of the mesoporosity of PMWW and PMFI

in sucrose hydrolysis reactions in an aqueous solvent have not been studied. We aim to reveal the catalytic performance of PMFI and PMWW zeolites in these reactions and to directly compare their catalytic performance to that of conventional microporous zeolite catalysts. The present study will lead to a systematic understanding of the effects of zeolite microenvironment (topology, mesoporosity, and acidity) on conversion of sucrose and other related biomass molecules under environmentally friendly conditions.

2. Experimental

2.1 Preparation of zeolite catalysts

The conventional microporous FER, MFI, MOR, BEA, and FAU with different acidity (Si/Al ratio) were purchased from Zeolyst. MWW and PMWW were derived from the same precursor, MWW (P). The hydrothermal synthesis of MWW (P) was carried out by using the method described by Corma *et al.*^{39,40} One portion of the crystalline product MWW (P) was dried and calcined to produce MWW. The other portion of MWW (P) was swollen according to the method developed by Maheshwari *et al.*,⁴¹ followed by pillaring of the swollen materials using the procedure reported by Barth *et al.*³⁸ The resulting solid was treated using the same conditions as those for MWW to produce PMWW. A multilamellar MFI was synthesized using the method reported by Ryoo and co-workers,⁴³ through a coherent assembly of the zeolite layer and the structure directing agent, a diquatery ammonium surfactant with a relatively long hydrocarbon chain. Pillaring of multilamellar MFI was done as reported by Na *et al.*⁴² to produce PMFI, using a similar pillaring procedure to that of swollen MWW (P). The as-synthesized MWW and MFI zeolites were ion-exchanged four times using 1 mol L⁻¹ aqueous NH₄NO₃ (weight ratio of zeolite to NH₄NO₃ solution = 1 : 10) at 353 K for 12 h and subsequently collected by vacuum filtration, washed with deionized (DI) water three times, and dried at 343 K overnight. No ion-exchange process was applied to the commercial zeolites since they were purchased in the NH₄⁺-form. All zeolite samples in their NH₄⁺-form were treated in dry air (100 mL min⁻¹, ultrapure, Airgas) by increasing the temperature from ambient temperature to 823 K at 1.45 K min⁻¹ and holding for 4 h to thermally decompose NH₄⁺ to NH₃ and H⁺. To differentiate the same type of zeolite with different Si/Al ratios, each catalyst is named by its structure type and Si/Al ratio in the remainder of this paper.

2.2 Textural and acidity property investigation

A scanning electron microscope (SEM) was employed for direct visualization of crystal morphologies of meso-/microporous and microporous zeolite catalysts. SEM images were collected on a JEOL 6500 SEM without crushing or a metal coating of the samples. Powder X-ray diffraction (XRD) patterns were collected on a Bruker AXS D5005 diffractometer using Cu-K α radiation. Nitrogen (N₂) adsorption-desorption measurements were carried out at 77 K on an Autosorb-iQ analyzer (Quantachrome Instruments). Prior to the measurement, samples were evacuated overnight at 573 K and 1 mmHg. Si and Al

contents were determined by inductively coupled plasma optical emission spectroscopy (ICP-OES, Galbraith Laboratories).

2.3 Catalytic hydrolysis of sucrose

The liquid phase catalytic hydrolysis of sucrose (Sigma-Aldrich, 99.5% purity) in DI water was carried out in a three-neck round-bottom flask (100 mL) equipped with a reflux condenser and heated in a temperature controlled oil bath under atmospheric pressure and magnetic stirring (1" stirring bar, 500 rpm stirring speed) conditions. The reaction scheme of sucrose hydrolysis is illustrated in Fig. 1. In a typical experiment, 20 mL of DI water was added to the desired amount (typically 0.2 g) of zeolite catalyst. The as-obtained mixture was maintained for 0.5 h under the required reaction temperature and stirring conditions and then 1.0 g of sucrose was added. This moment of sucrose addition was considered as the initial reaction time. Liquid samples were withdrawn at regular intervals and analyzed by a high performance liquid chromatograph (Agilent 1100 HPLC) equipped with a Bio-Rad Aminex HPX-87H column connected to an autosampler and a refractive index detector to calibrate and separate the reactants and products. During the measurement, the column was kept at 333 K with 0.005 mol L⁻¹ sulfuric acid at a flow rate of 0.5 mL min⁻¹ as the mobile phase. Under these analysis conditions, the hydrolysis of sucrose in a sulfuric acid eluent was less than 0.2%, showing that the HPLC analysis method did not influence the reaction results. The influence of external mass transfer limitations on the reaction rates was ruled out by running the reactions at a high enough stirring speed (500 rpm), showing that a further increase in the stirring speed did not enhance the reaction rate anymore. In the examined temperature interval, absence of products from consecutive reactions of glucose was confirmed by running a control experiment using glucose as the reactant. Conversion of fructose by the following series reactions was observed by HPLC analysis. Zeolite colorization was not observed in the studied reaction conditions.

3. Results and discussion

3.1 Topological properties of zeolite catalysts

Small, medium, and large pore zeolites are classified according to their pore openings that are 8-, 10-, and 12-membered rings

(MR), respectively.^{46,47} Table 1 summarizes the types of zeolites and graphical representation of the pore systems of each zeolite catalyst. FER zeolite contains one-dimensional channels of 10-MR (0.42 × 0.54 nm) and one-dimensional channels of 8-MR (0.35 × 0.48 nm) that are perpendicularly intersected. MFI zeolite consists of two interconnected 10-MR channel systems: one is straight running along the *b*-axis direction (0.53 × 0.56 nm) and the other is zigzag running parallel to the *a*-axis direction (0.51 × 0.55 nm). The PMFI contains mesopores created by the inorganic pillar species sitting between MFI layers, parallel to the zigzag channels and perpendicular to the straight channels within the layers. MWW structure contains two independent pore systems. One system is defined by sinusoidal 10-MR channels with dimensions of 0.41 × 0.51 nm and the other system consists of supercages delimited by 12-MR channels with dimensions of 0.71 × 0.71 × 1.81 nm. The consecutive supercages are connected through slightly distorted elliptical 10-MR windows (0.40 × 0.55 nm). The PMWW was created by pillaring the MWW layers by SiO₂, containing the 10-MR sinusoidal channels and hourglass shaped pores (half of the supercages in MWW) within the intact layers and mesopores between the layers. Table 1 also shows that MOR zeolite has the 8-MR pocket (0.34 × 0.48 nm) and 12-MR (0.7 × 0.65 nm) channel systems, with the 8-MR pockets sitting in the walls of 12-MR channels. A BEA zeolite structure consists of 12-MR straight channels of a free aperture of 0.66 × 0.67 nm viewed along the *a*-axis and 12-MR zigzag channels of 0.56 × 0.56 nm viewed along the *c*-axis. FAU zeolite contains 12-MR pore mouths (0.74 × 0.74 nm) that are 3-dimensionally connected with internal supercages (~1.3 nm). The topological analysis above indicates that FER and MFI are medium-pore zeolites, MOR, MWW, BEA, and FAU are large-pore zeolites, and PMWW and PMFI are mesoporous zeolites, respectively.

3.2 Morphology of zeolite catalysts

Fig. 2 shows the SEM images of zeolite catalysts used in the sucrose hydrolysis reactions. FER (FER-28) contains flake-like particles that form large aggregates, as shown in Fig. 2(a). The MFI (MFI-12 and MFI-40), MOR (MOR-45), BEA (BEA-12, BEA-19, and BEA-100), and FAU (FAU-15 and FAU-40) zeolites with no specific particle sizes due to their broad range of sizes are shown in Fig. 2(b)–(c), (e), (h)–(j), (k)–(l), respectively.

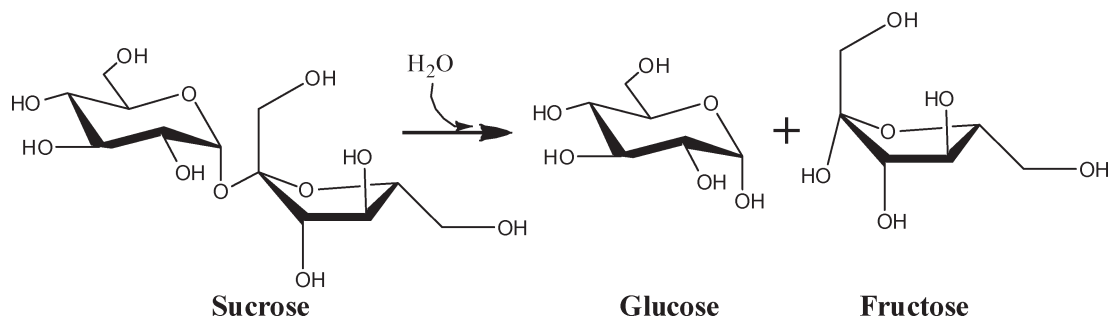
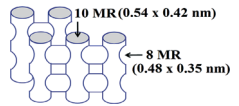
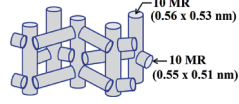
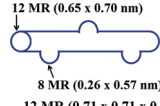
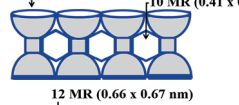
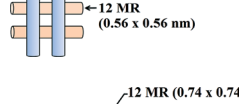
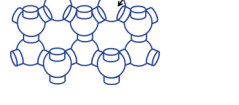
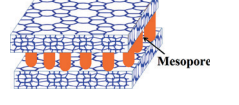
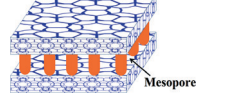


Fig. 1 Scheme showing the hydrolysis of sucrose to glucose and fructose in an aqueous solution.

Table 1 Topology and graphical representation of pore systems of the medium-pore, large-pore, and mesoporous zeolite catalysts used in the sucrose hydrolysis reactions

Zeolite		Si/Al ratio	Pore structure		Graphical representation of pore topology
			Pore shape	Pore size (nm)	
Medium-pore	FER	28	8 MR	0.35×0.48	
			10 MR	0.42×0.54	
	MFI	12 40 70	10 MR 10 MR	0.51×0.55 0.53×0.56	
Large-pore	MOR	45	8 MR	0.34×0.48	
			12 MR	0.65×0.7	
	MWW	20 30	10 MR	0.41×0.55	
			10 MR	0.41×0.51	
	BEA	12 19 100	Supercage	0.71×1.82	
			Side pocket	$0.71 d^a \times 0.9 h^b$	
12 MR			0.56×0.56		
FAU	15 40	12 MR	0.74×0.74		
		12 MR	0.74×0.74		
Mesopore	PMFI	70	10 MR	0.51×0.55	
		150	10 MR	0.53×0.56	
		200	Mesopore ^c	2.8	
PMWW	30	10 MR	0.41×0.51		
		Supercage	0.71×1.82		
		Side pocket	$0.71 d^a \times 0.9 h^b$		
			Mesopore ^c	1.8	

^a d represents "diameter". ^b h represents "height". ^c The mesopore size was determined from the N_2 adsorption branch by using the BJH model.

The synthesized MFI (MFI-70) zeolite has a uniform particle size of ~ 200 nm (Fig. 2(d)). The PMFI (PMFI-70, PMFI-150, and PMFI-200) zeolites in Fig. 2(m)–(o) are composed of aggregated platelet-like particles, similar to the PMFI reported by Na *et al.*⁴² The synthesized MWW (MWW-20 and MWW-30) zeolites crystallize as thin rounded flakes, which are 500–1000 nm in diameter and 50–100 nm in thickness, as shown in Fig. 2(f)–(g). PMWW (PMWW-30) resembles the disc-like crystal morphology of MWW, as evidenced by comparing the morphology of PMWW in Fig. 2(p) to that of MWW. The SEM images reveal that no obvious trend on zeolite geometrical properties is observable in all the investigated catalysts. The trends of catalytic behaviors of the zeolite catalysts, discussed below, are predominately dominated by the zeolite microenvironments of the catalysts. The XRD patterns of the synthesized MWW, MFI, PMWW, and PMFI confirm that the samples are highly crystalline and the data have been reported in our previous publication.⁴⁴

3.3 N_2 adsorption–desorption isotherm analysis

N_2 adsorption–desorption measurements were used to reveal the porosity features of the medium-pore, large-pore, and mesoporous zeolite catalysts. Table 2 summarizes the micropore volume, cumulative pore volume, and Brunauer–Emmett–Teller (BET) surface area of each catalyst analyzed from N_2 adsorption–desorption isotherms. Among all the investigated microporous catalysts, FAU-type zeolites have the highest surface area, cumulative pore volume, and micropore volume, followed by the BEA-type zeolites. MWW-, MOR-, and MFI-type zeolites have similar surface areas and micropore and cumulative pore volumes, all of which are smaller than those of FAU and BEA zeolites. FER has the lowest surface area and cumulative pore volume among all the investigated microporous zeolites. The meso-/microporous PMFI and PMWW zeolites have similar surface areas and cumulative

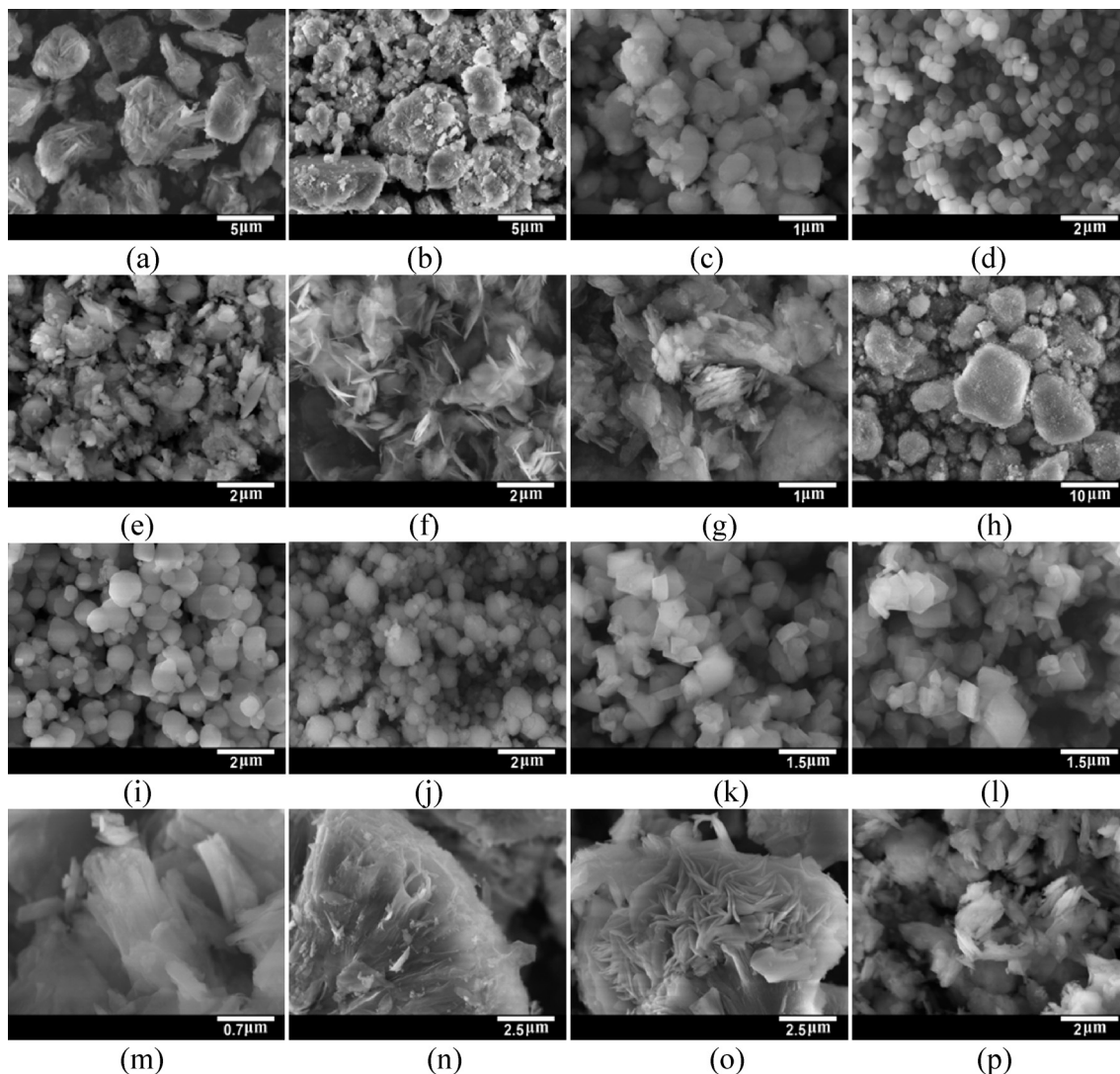


Fig. 2 SEM images of (a) FER-28, (b) MFI-12, (c) MFI-40, (d) MFI-70, (e) MOR-45, (f) MWW-20, (g) MWW-30, (h) BEA-12, (i) BEA-19, (j) BEA-100, (k) FAU-15, (l) FAU-40, (m) PMFI-70, (n) PMFI-150, (o) PMFI-200, and (p) PMWW-30.

pore volumes that are larger than those of microporous BEA but smaller than those of FAU zeolites. The acidity of the zeolite catalysts does not influence their porosity properties, as shown by the similar surface areas and pore volumes across the same type of zeolites with different Si/Al ratios. The surface areas and porosities of these zeolites are consistent with their topological properties discussed in section 3.1.

3.4 Sucrose hydrolysis reaction

In water solvent, sucrose (A) was consumed simultaneously *via* hydrolysis ($A + H_2O \rightarrow B + C$) reactions to form fructose (B) and glucose (C). Because an excess amount of water was used, the hydrolysis reaction can be approximated as pseudo-first order in the limiting reactant A, sucrose. The rate equation is

$$\frac{dC_C}{dt} = k_{\text{hydro}} M_B C_A \quad (1)$$

where C_C is the glucose concentration in solution (mol L^{-1}), t is the reaction time (s), k_{hydro} is the specific rate constant (per Brønsted acid site, $[\text{mol H}^+]^{-1} \text{s}^{-1}$), M_B (mol H^+) is the total moles of Brønsted acid sites present in the batch reactor, and C_A is the sucrose concentration in solution (mol L^{-1}). The number of acid sites of each catalyst is shown in Table 2. By integrating eqn (1), the rate equation becomes

$$\ln\left(\frac{C_A^0}{C_A}\right) = -k_{\text{hydro}} M_B t \quad (2)$$

where C_A^0 is the initial sucrose concentration in solution (mol L^{-1}).

The profiles of sucrose conversion as a function of reaction time and $\ln(C_A^0/C_A)$ as a function of reaction time in the hydrolysis of sucrose for different temperatures over the investigated catalysts with variable micropore topology, mesoporosity, and acidity are reported in Fig. S1.† The linear

Table 2 Acidity and porosity characteristics of the medium-pore, large-pore, and mesoporous zeolites used in sucrose hydrolysis reactions

Zeolite		Si/Al ratio ^a	Number of Brønsted acid sites ^b (mmol g ⁻¹)	Cumulative pore vol ^c (cc g ⁻¹)	Micropore vol ^d (cc g ⁻¹)	BET surface area ^e (m ² g ⁻¹)
Medium-pore	FER	28	0.575	0.144	0.103	368
	MFI	12	1.282	0.168	0.132	410
		40	0.406	0.199	0.137	466
		70	0.235	0.173	0.136	427
Large-pore	MOR	45	0.362	0.214	0.162	552
	MWW	20	0.794	0.196	0.143	384
		30	0.538	0.210	0.120	442
		100	0.165	0.267	0.169	662
	FAU	15	1.042	0.350	0.198	871
		40	0.407	0.359	0.201	877
		200	0.083	0.307	0.125	642
	Mesopore	PMFI	70	0.235	0.349	0.118
150			0.110	0.317	0.121	674
200			0.083	0.307	0.125	642
	PMWW	30	0.538	0.359	0.131	771

^a Determined from elemental analysis (ICP-OES, Galbraith Laboratories). ^b Calculated based on Si/Al ratio in each sample. ^c Cumulative pore volume determined using the Saito-Foley method. ^d Micropore volume determined by the *t*-plot method. ^e Surface area calculated from the multi-point BET model.

trends in $\ln(C_A^0/C_A)$ as a function of reaction time are satisfactory in all the cases, confirming that the sucrose hydrolysis is the pseudo-first-order reaction. From the observed rate constants ($k_{\text{hydro}}M_B$), calculated from the slope of the lines in Fig. S1,† k_{hydro} can be obtained for each catalyst at a designated reaction temperature. The as-obtained k_{hydro} values have been listed in Table S1 with their confidence intervals.†

The temperature dependence of the rate constants of the sucrose hydrolysis over the zeolite catalysts was evaluated by the Arrhenius plot (the natural logarithm of regressed rate constants *versus* the inverse temperature) approach (refer to Fig. S2 in the ESI†) to assess the kinetic parameters of the reaction. The slope of the Arrhenius plot was used to calculate the measured reaction activation energies (ΔE_{meas} , kJ mol⁻¹). The Eyring equation (eqn (3)) was used to calculate the measured reaction entropies (ΔS_{meas} , J mol⁻¹ K⁻¹),

$$\ln(k_{\text{hydro}}) = \ln\left(\frac{k_B T}{h}\right) + \left(-\frac{1}{RT}(\Delta H_{\text{meas}} - T\Delta S_{\text{meas}})\right) \quad (3)$$

where k_B is the Boltzmann constant (m² kg s⁻² K⁻¹), T is the absolute temperature (K), h is the Planck's constant (m² kg s⁻¹), R is the ideal gas constant (J mol⁻¹ K⁻¹), and ΔH_{meas} is the measured reaction enthalpy (kJ mol⁻¹), respectively. From eqn (3), the measured reaction entropy equals $R[\text{intercept in Arrhenius plot} - \ln(k_B T/h)]$. Below, the effect of zeolite micropore topology, acidity, and mesoporosity on the hydrolysis of sucrose reactions and the corresponding kinetic parameters (measured activation energies and entropies) are discussed in sequence.

3.4.1 Zeolite micropore topology effect. Fig. 3 shows the rate constants (k_{hydro}) of sucrose hydrolysis at 352 K over zeolites with similar Si/Al ratio but different micropore topology. The sucrose hydrolysis rate on FER-28 and MWW-30 (with a similar Si/Al ratio of ~30) increases with increasing

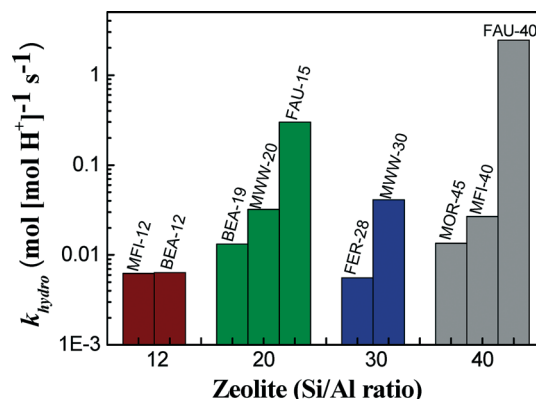


Fig. 3 Rate constant of sucrose hydrolysis over zeolite catalysts with a similar Si/Al ratio and different micropore topology ($T = 352$ K).

zeolite micropore sizes from 8-MR \times 10-MR channels in FER to 10-MR channels \times 12-MR supercages in MWW. The increase in reaction rate with increasing micropore sizes of zeolites is also observed for the hydrolysis reaction over zeolite MFI, MOR, and FAU with a Si/Al ratio of ~40, zeolite MFI and BEA with a Si/Al ratio of ~12, and BEA, MWW, and FAU with a Si/Al ratio of ~20, respectively. These results clearly indicate that the hydrolysis of sucrose preferentially occurs in large-pore zeolites. In contrast, spatial constraints imposed by small pores of zeolites may mainly allow surface catalysis to occur.

The difference in activity of the zeolite catalysts can be understood from the molecular size of sucrose and the pore size of the zeolite catalysts. In the aqueous solution, the sucrose molecule is characterized by an approximately spherical shape with a relevant diameter of ~0.88 nm.²⁹ Although the largest pore size of the investigated catalysts is 0.74 nm in the FAU catalyst, the sucrose molecule can enter the zeolite pore by adopting a more elliptic form. The larger pore

sizes of the catalyst, the easier it is for the sucrose molecules to enter the zeolite micropore. As a result, the labile protons on the active sites of the catalysts have more mobility to reach the oxygen of the acetalic bond in sucrose and to promote the hydrolysis reaction. The FAU-type zeolite has the highest activity in the investigated catalysts, followed by BEA- and MWW-type zeolites, which are consistent with their topology features and porosity properties of the catalysts shown in Tables 1 and 2, respectively. MOR is ascribed to the large-pore zeolite category. The pore channels of MOR, however, run along a one-dimensional direction. MFI belongs to the medium-pore zeolite category, while the 10-MR channels run along 3-dimensional directions that may facilitate the transport of sucrose molecules in the pore systems compared to MOR-type catalysts. As a result, the MFI has comparable reaction activity in sucrose hydrolysis to that of the large-pore MOR zeolite. FER consists of 8-MR \times 10-MR pore channels, the smallest pore sizes among the investigated catalysts. Therefore, the lowest reaction rate of sucrose hydrolysis is observed for the FER-type zeolite. The present study systematically examined the effect of zeolite micropore topology on the reaction rate of sucrose hydrolysis, showing a trend of FER < MOR ~ MFI < BEA ~ MWW < FAU.

3.4.2 Zeolite acidity effect. Fig. 4 shows the rate constants of the hydrolysis of sucrose over MFI, BEA, MWW, and FAU zeolites with variable Si/Al ratios. The rate constant per acid site generally increases sharply with increasing Si/Al ratio to ~50 in each type of catalyst and then reaches a plateau when the Si/Al ratio increases further to ~100, as shown in BEA-type zeolite catalysts. These data are consistent with that of hydrolysis of sucrose on FAU zeolite catalysts reported by Buttersack *et al.*²⁸ It has been shown that the catalytic activity of FAU zeolite increased strongly with increasing Si/Al ratio from 27 to 55 and then slightly with Si/Al ratio from 55 to 110. The present study indicates that this catalytic behavior is generalizable to MFI-, BEA-, and MWW-type zeolite catalysts. Fig. 4 also indicates that the zeolite activity trend of MFI < BEA ~ MWW < FAU in sucrose hydrolysis reactions is independent of their Si/Al ratio. The comparison of the

zeolite micropore topology and acidity effects on the sucrose hydrolysis reactions shows that zeolite topological properties play a more important role in determining the zeolite catalytic activity.

The changes in the catalytic activity as a function of the zeolite acidity (Si/Al ratios) can be understood from the interactions of sucrose and the active sites in the zeolite, which is related to the local concentration of sucrose and acid sites in the zeolite catalysts. The variation on the Si/Al ratios changes the hydrophilicity–hydrophobicity balances of the zeolite catalysts.⁴⁸ A higher Si/Al ratio induces more hydrophobicity of the zeolites and thus stronger adsorption of saccharide molecules onto zeolite catalysts. The adsorption of saccharide molecules on the zeolites can be expressed by the empirical correlation, $K = b - a \ln(x)$, where K is the adsorption equilibrium constant, a and b are the parameters specifying the hydrophilicity–hydrophobicity of the adsorbed saccharides, and x is the fraction of ionic sites in the zeolites.^{49,50} An increase in Si/Al ratio of zeolites results in a decrease in x and an increase in the adsorption equilibrium constant of sucrose molecules, and the resultant increased affinity to the zeolite catalysts. Higher affinity of the sucrose molecule towards the zeolite with higher Si/Al ratios was confirmed for the Na⁺-form FAU zeolites.⁴⁹ The increase in affinity of the sucrose molecules towards the zeolites with higher Si/Al ratios results in the enhancement of catalytic activity per acid site of the catalysts.

3.4.3 Zeolite mesoporosity effect. Fig. 5 shows the effect of the zeolite mesoporosity on the reaction rate of sucrose hydrolysis. Two pairs of zeolite catalysts, MWW-30 and PMWW-30, MFI-70 and PMFI-70, respectively, were employed for this study. The inclusion of mesopores by pillaring the lamellar MWW and lamellar MFI resulted in the enhancement on the reaction rates by a factor of ~2, consistent with their porosity properties discussed in section 3.2. The increase in the reaction rates with increasing zeolite mesoporosity may result from the enhanced acid site accessibility and mass transport in meso-/microporous PMWW and PMFI

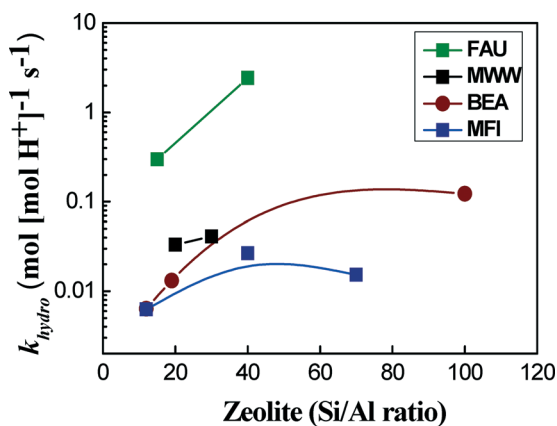


Fig. 4 Rate constant of sucrose hydrolysis over MFI, BEA, MWW, and FAU with different Si/Al ratios ($T = 352$ K).

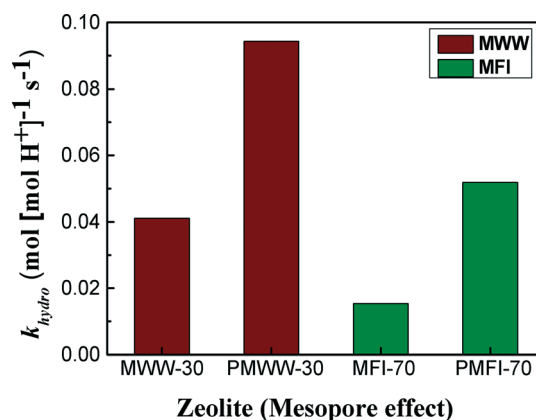


Fig. 5 Rate constant of sucrose hydrolysis over MWW, PMWW, MFI, and PMFI zeolite catalysts ($T = 352$ K). (MWW and PMWW both have Si/Al of 30; MFI and PMFI both have Si/Al of 70.)

catalysts. Our previous studies on Brønsted acid site accessibility to bulky molecules by 2,6-di-tertbutyl pyridine (DTBP) titrations has shown that PMWW and PMFI zeolites had ~10 times higher accessibility to DTBP molecules compared to microporous MFI and MWW zeolites.⁴⁴ Also, the PMWW and PMFI catalysts showed much more efficient catalysis in diffusion constrained catalytic reactions when the self-etherification of benzyl alcohol and alkylation of mesitylene were used as the probe reactions.⁴⁵

The comparison of sucrose hydrolysis reaction rates of the meso-/microporous zeolites (PMFI and PMWW) and the large-pore zeolites (BEA and FAU) in Table S1† shows that the meso-/microporous zeolites have a comparable activity to that of BEA-type zeolites but a lower activity (~1 order of magnitude) than that of FAU-type zeolites. This result indicates that the hydrolysis of sucrose is dominated by the zeolite microporous topological properties. PMFI and PMWW contain mesopores between the zeolitic layers and micropores within the zeolite layers. The pillaring causes the increase in mesoporosity but not in zeolite microporosity. Table 2 shows that PMFI and PMWW have similar micropore volumes to those of MFI and MWW zeolite catalysts. The active sites in mesopores, however, might experience the sucrose molecules with a large hydration layer, which limit the reaction rate in comparison with large micropores in FAU that might only contain one water molecule around each sucrose molecule to facilitate the reaction rate.²⁸ The comparison of the zeolite catalyst with Amberlyst-15, the industrial standard catalyst, shows that Amberlyst-15 has comparable reaction rate constants to BEA zeolite, as illustrated in Table S1 and Fig. S1 in the ESI.†

Fig. 6 shows the acidity dependence of the sucrose hydrolysis reaction in meso-/microporous zeolites. Similar to that of medium- and large-pore conventional microporous zeolite catalysts, the activity per acid site increases with increasing Si/Al ratio from 70 to 150. The further increase in Si/Al ratio to ~200, however, decreases the activity per acid site. A possible explanation is that the hydrophobicity of the zeolite with very high Si/Al ratios restricts the access of the water

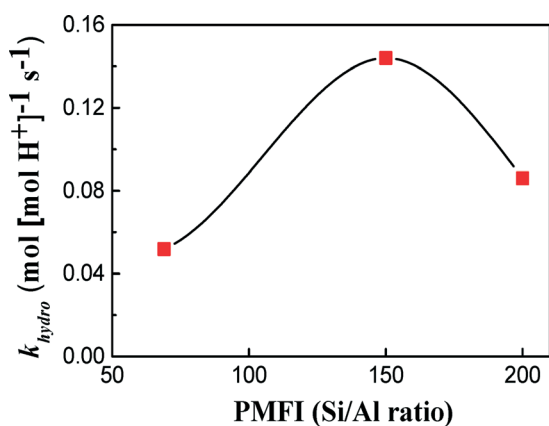


Fig. 6 Rate constant of sucrose hydrolysis over mesoporous PMFI zeolites with different Si/Al ratios ($T = 352$ K).

molecules to the active sites, considering that the hydrolysis of sucrose is conducted in aqueous and mild reaction temperature conditions.

3.4.4 Assessment of kinetic parameters. Fig. 7 compares the activation energies (ΔE_{meas}) and entropies (ΔS_{meas}) for the sucrose hydrolysis over all the investigated zeolite catalysts. Activation energies are comparable for the medium-pore, large-pore, and mesoporous zeolites, in the range of 102–138 kJ mol⁻¹ as shown in Fig. 7(a). The activation energies are consistent with those of sucrose hydrolysis in FAU zeolites reported by Buttersack²⁸ and the more general hydrolysis of other disaccharides in acid solutions. The activation entropies, shown in Fig. 7(b), increase from 15 to 135 J mol⁻¹ K⁻¹ as the zeolite category changes from the medium-pore to large-pore zeolites. The increases in Si/Al ratios in the same type of zeolite resulted in the increase in activation entropies by a factor ~2. The presence of mesopores in the meso-/microporous PMWW and PMFI zeolite leads to the increase in activation entropies by a factor ~1.5 compared to their microporous analogues. The changes in

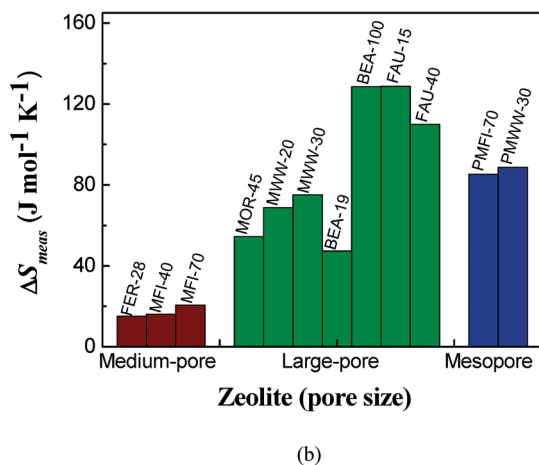
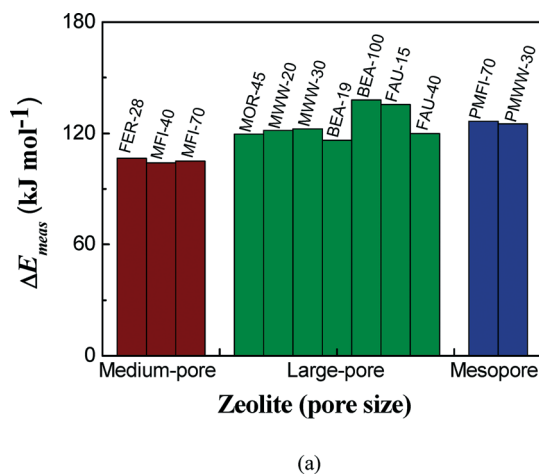


Fig. 7 The measured activation energy (ΔE_{meas}) (a) and measured entropy (ΔS_{meas}) at 352 K (b) of sucrose hydrolysis reactions over zeolite catalysts with different micropore topology, mesoporosity, and acidity (Si/Al ratio).

the reaction entropies are consistent with the variation on the zeolite microenvironment (micropore topology, mesoporosity, and acidity), indicating that the hydrolysis of sucrose over zeolite catalysts is primarily driven by the activation entropies, in accordance with reports by BeMiller *et al.*⁵¹ Adsorption and diffusion should contribute to the observed reaction kinetics. The absence of adsorption equilibrium constants and diffusion coefficients of sucrose from each zeolite catalyst limits the further analysis on the intrinsic kinetic parameters of sucrose hydrolysis in the microenvironments of the zeolite catalysts.

4. Conclusions

The catalytic consequences of micropore topology, mesoporosity, and acidity on the hydrolysis of sucrose over zeolite catalysts were examined systematically. The calculated rate constants, activation energies, and entropies of the hydrolysis reactions over each catalyst have been used to quantify the effects of microenvironment of the catalysts on the reaction. The results confirmed that the large-pore zeolites have higher activity than medium-pore zeolites. Meso-/microporous zeolites have higher activity compared to their microporous analogues, possibly due to the mitigated diffusion constraints and enhanced acid site accessibility, but still lower than that of large-pore FAU zeolites. The activity per acid site of the zeolite catalysts was found to increase with the decreasing amount of acid sites in each zeolite. The further decrease in active site content resulted in reduced activity per acid site. The comparison of the effects of zeolite microenvironments on the hydrolysis of sucrose indicates a trend of micropore topology > acidity > mesoporosity. Similar apparent activation energies are observed across all the catalysts, while the apparent entropies vary with zeolite topology and acidity. This result indicates that activation of sucrose over the zeolite catalysts is driven primarily by the reaction entropies, which are influenced by the zeolite topological and acidity properties.

Acknowledgements

The authors gratefully acknowledge the support from the PI's start-up fund at the University of Maryland, College Park. Portions of this work were supported by the ACS-Petroleum Research Fund (ACS-PRF). We acknowledge the support of the Maryland NanoCenter and its NispLab. The NispLab is supported in part by the NSF as a MRSEC Shared Experimental Facility. Y. H. acknowledges the Chinese Scholarship Council (CSC) and Prof. Xiaoqian Ma at the South China University of Technology.

References

- 1 M. A. Rubio Rodríguez, J. De Ruyck, P. Roque Díaz, V. K. Verma and S. Bram, *Appl. Energy*, 2011, **88**, 630.
- 2 W. P. Nel and C. J. Cooper, *Energy Policy*, 2009, **37**, 166.
- 3 C. H. Zhou, X. Xia, C. X. Lin, D. S. Tong and J. Beltramini, *Chem. Soc. Rev.*, 2011, **40**, 5588.
- 4 G. W. Huber, S. Iborra and A. Corma, *Chem. Rev.*, 2006, **106**, 4044.
- 5 S. Peat, *Annu. Rev. Biochem.*, 1946, **15**, 75.
- 6 A. Corma, S. Iborra and A. Velty, *Chem. Rev.*, 2007, **107**, 2411.
- 7 A. Pessoa-Jr, I. C. Roberto, M. Menossi, R. R. Dos Santos, S. Ortega Fikho and T. C. V. Penna, *Appl. Biochem. Biotechnol.*, 2005, **121**, 59.
- 8 T. Hasunuma, F. Okazaki, N. Okai, K. Y. Hara, J. Ishii and A. Kondo, *Bioresour. Technol.*, 2013, **135**, 513.
- 9 P. Hasal, V. Vojtisek, A. Cejkova, P. Kleczek and O. Kofronova, *Enzyme Microb. Technol.*, 1992, **14**, 221.
- 10 T. A. Lloyd and C. E. Wyman, *Bioresour. Technol.*, 2005, **96**, 1967.
- 11 S. Bower, R. Wickramasinghe, N. J. Nagle and D. J. Schell, *Bioresour. Technol.*, 2008, **99**, 7354.
- 12 M. Marzo, A. Gervasini and P. Carniti, *Carbohydr. Res.*, 2012, **347**, 23.
- 13 A. Abbadi, K. F. Gotlieb and H. van Bekkum, *Starch/Stärke*, 1998, **50**, 23.
- 14 A. Onda, T. Ochi and K. Yanagisawa, *Green Chem.*, 2008, **10**, 1033.
- 15 J. A. Tian, C. Y. Fan, M. X. Cheng and X. H. Wang, *Chem. Eng. Technol.*, 2011, **34**, 482.
- 16 M. M. Nasef, H. Saidi and M. M. Senna, *Chem. Eng. J.*, 2005, **108**, 13.
- 17 P. L. Dhepe, M. Ohashi, S. Inagaki, M. Ichikawa and A. Fukuoka, *Catal. Lett.*, 2005, **102**, 163.
- 18 B. Foche, A. Marzetti, P. L. Beltrame and P. Carniti, in *Biosynthesis and biodegradation of cellulose*, Marcel Dekker, New York, 1991.
- 19 P. Carniti, P. L. Beltrame, D. Guardione, B. Foche and A. Marzetti, *Biotechnol. Bioeng.*, 1991, **37**, 575.
- 20 D. S. Pito, I. M. Fonseca, A. M. Ramos, J. Vital and J. E. Castanheiro, *Bioresour. Technol.*, 2009, **100**, 4546.
- 21 D. S. Pito, I. M. Fonseca, A. M. Ramos, J. Vital and J. E. Castanheiro, *Chem. Eng. J.*, 2012, **184**, 347.
- 22 P. Lanzafame, D. M. Temi, S. Perathoner, A. N. Spadaro and G. Centi, *Catal. Today*, 2012, **179**, 178.
- 23 A. Takagaki, C. Tagusagawa and K. Domen, *Chem. Commun.*, 2008, 5363.
- 24 A. Onda, *J. Jpn. Pet. Inst.*, 2012, **55**, 73.
- 25 S. Lima, M. M. Antunes, A. Fernandes, M. Pillinger, M. F. Ribeiro and A. A. Valente, *Molecules*, 2010, **15**, 3863.
- 26 C. Moreau, R. Durand, J. Duhamet and P. Rivalier, *J. Carbohydr. Chem.*, 1997, **16**, 709.
- 27 M. S. Holm, S. Saravanamurugan and E. Taarning, *Science*, 2010, **328**, 602.
- 28 C. Buttersack and D. Laketic, *J. Mol. Catal.*, 1994, **94**, L283.
- 29 K. Kiyosawa, *Bull. Chem. Soc. Jpn.*, 1988, **61**, 633.
- 30 C. Moreau, R. Durand, F. R. Alies, M. Cotillon, T. Frutz and M. A. Theoleyre, *Ind. Crops Prod.*, 2000, **11**, 237.
- 31 J. Weitkamp, *Solid State Ionics*, 2000, **131**, 175.
- 32 K. Na, M. Choi and R. Ryoo, *Microporous Mesoporous Mater.*, 2013, **166**, 3.

- 33 J. Čejka, G. Centi, J. Perez-Pariente and W. J. Roth, *Catal. Today*, 2012, **179**, 2.
- 34 R. Chal, C. Gérardin, M. Bulut and S. van Donk, *ChemCatChem*, 2011, **3**, 67.
- 35 M. S. Holm, E. Taarning, K. Egeblad and C. H. Christensen, *Catal. Today*, 2011, **168**, 3.
- 36 L. P. Zhou, M. T. Shi, Q. Y. Cai, L. Wu, X. P. Hu, X. M. Yang, C. Chen and J. Xu, *Microporous Mesoporous Mater.*, 2013, **169**, 54.
- 37 H. Iloukhani, S. Azizian and N. Samadani, *React. Kinet. Catal. Lett.*, 2001, **72**, 239.
- 38 J. O. Barth, A. Jentys, J. Kornatowski and J. A. Lercher, *Chem. Mater.*, 2004, **16**, 724.
- 39 A. Corma, V. Fornes, S. B. Pergher, T. L. M. Maesen and J. G. Buglass, *Nature*, 1998, **396**, 353.
- 40 M. K. R. Rubin, Composition of synthetic porous crystalline material, its synthesis and use, *US Patent No. 49454325*, 1990.
- 41 S. Maheshwari, E. Jordan, S. Kumar, F. S. Bates, R. L. Penn, D. F. Shantz and M. Tsapatsis, *J. Am. Chem. Soc.*, 2008, **130**, 1507.
- 42 K. Na, M. Choi, W. Park, Y. Sakamoto, O. Terasaki and R. Ryoo, *J. Am. Chem. Soc.*, 2010, **132**, 4169.
- 43 M. Choi, K. Na, J. Kim, Y. Sakamoto, O. Terasaki and R. Ryoo, *Nature*, 2009, 461.
- 44 D. Liu, A. Bhan, M. Tsapatsis and S. Al Hashimi, *ACS Catal.*, 2011, **1**, 7.
- 45 X. Y. Zhang, D. X. Liu, D. D. Xu, S. Asahina, K. A. Cychosz, K. V. Agrawal, Y. Al Wahedi, A. Bhan, S. Al Hashimi, O. Terasaki, M. Thommes and M. Tsapatsis, *Science*, 2012, **336**, 1684.
- 46 C. Baerlocher, W. M. Meier and D. H. Olson, *Atlas of Zeolite Framework Types*, Elsevier, Amsterdam, 5th edn, 2001.
- 47 <http://izasc.ethz.ch/fmi/xsl/IZA-SC/ft.xsl>.
- 48 K. K. Unger, U. R. Kittelmann and W. K. Kreis, *J. Chem. Technol. Biotechnol.*, 1981, **31**, 435.
- 49 C. Buttersack, W. Wach and K. Buchholz, *J. Phys. Chem.*, 1993, **97**, 11861.
- 50 C. Buttersack, W. Wach and K. Buchholz, in *Zeolites and Related Microporous Materials: State of the Art 1994*, Elsevier Science Publ. BV, Amsterdam, 1994, vol. 84, p. 1363.
- 51 J. N. BeMiller, *Adv. Carbohydr. Chem.*, 1967, **22**, 25.